A Universal Fuzzy Logic Optical Water Type Scheme for the Global Oceans

Tianxia Jia [1,2], Yonglin Zhang [1], Rencai Dong [1,*]

[1] State Key Laboratory of Urban and Regional Ecology, Research Center for Eco-environmental Sciences, Chinese Academy of Sciences, Beijing 100085, China;

[2] University of Chinese Academy of Sciences, Beijing 100049, China

* Correspondence author at: State Key Laboratory of Urban and Regional Ecology, Research Center for Eco-environmental Sciences, Chinese Academy of Sciences, Beijing 100085, China.

E-mail address: dongrencai@rcees.ac.cn (R. Dong)

Supplementary Materials

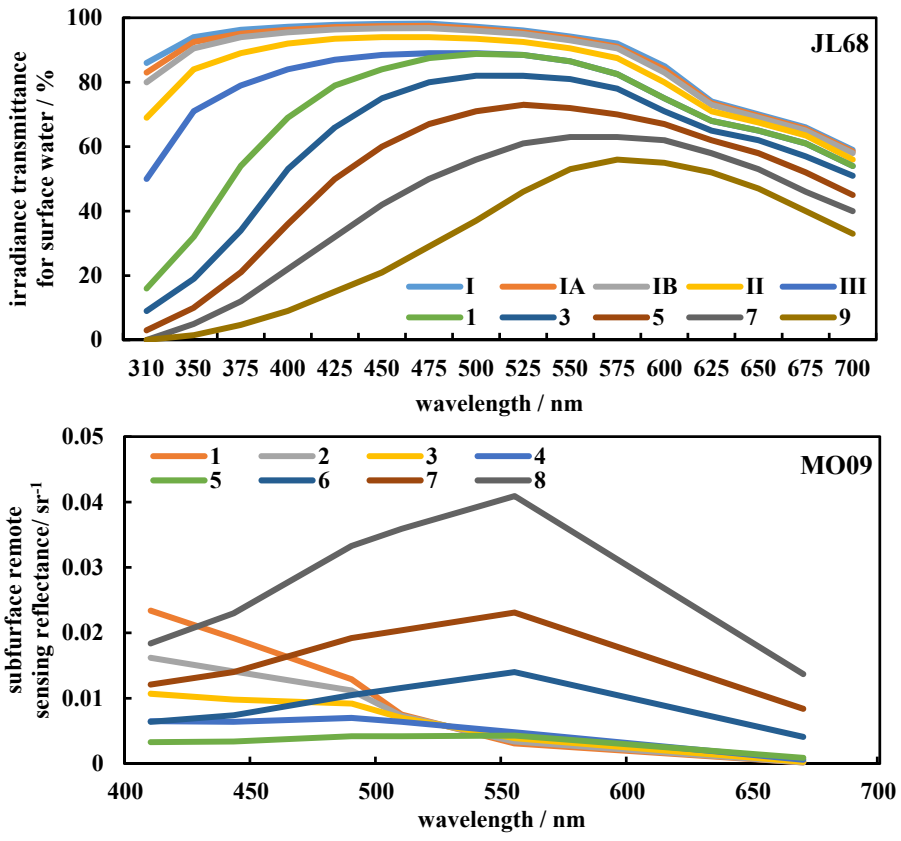

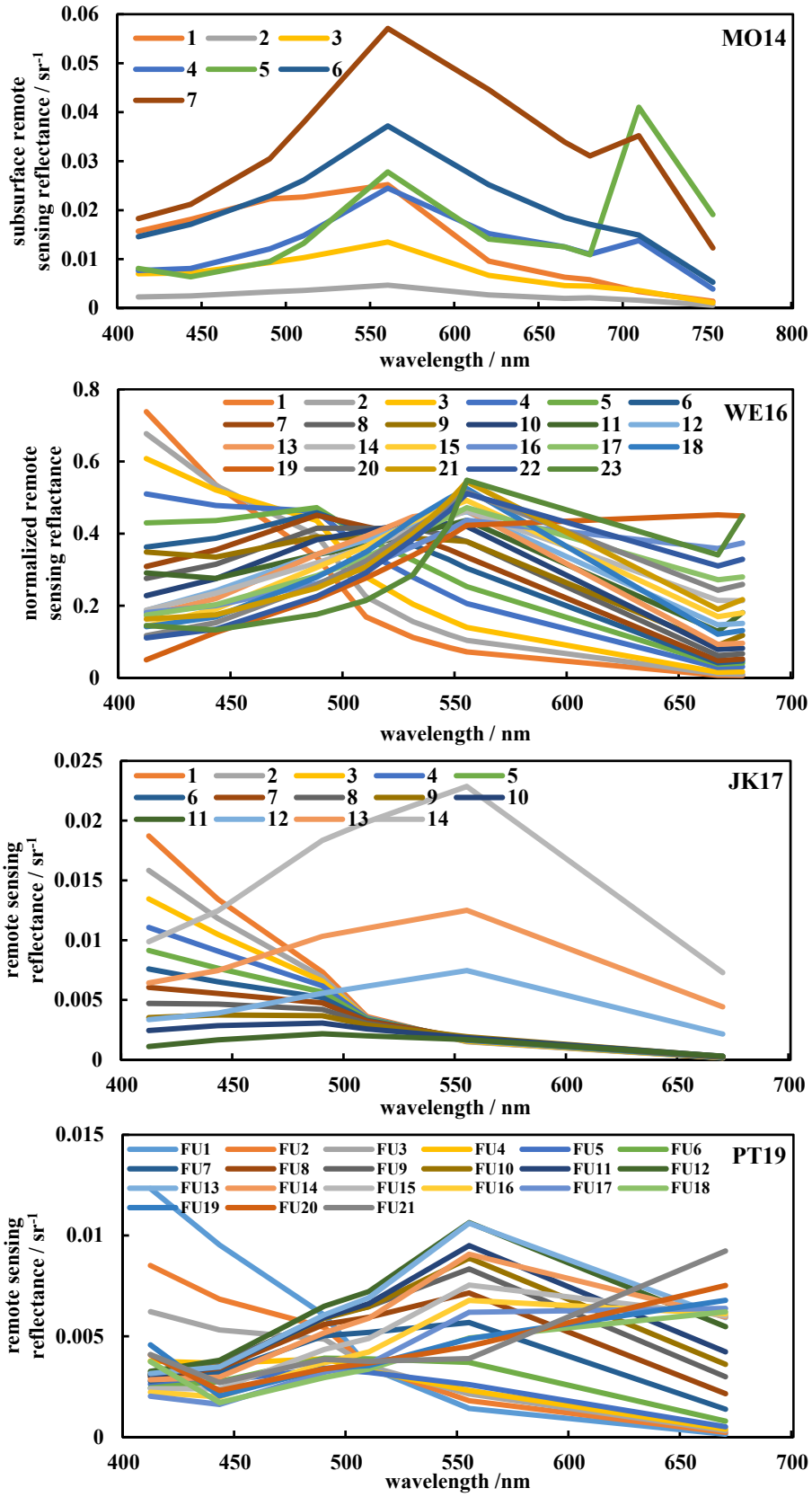
MO14
1
2
3
4
5
6
7
subsurface remote sensing reflectance / sr-1
wavelength / nm
WE16
normalized remote sensing reflactance
wavelength / nm
JK17
remote sensing reflectance / sr-1
wavelength / nm
PT19
FU1
FU2
FU3
FU4
FU5
FU6
FU7
FU8
FU9
FU10
FU11
FU12
FU13
FU14
FU15
FU16
FU17
FU18
FU19
FU20
FU21
remote sensing reflectance / sr-1
wavelength /nm

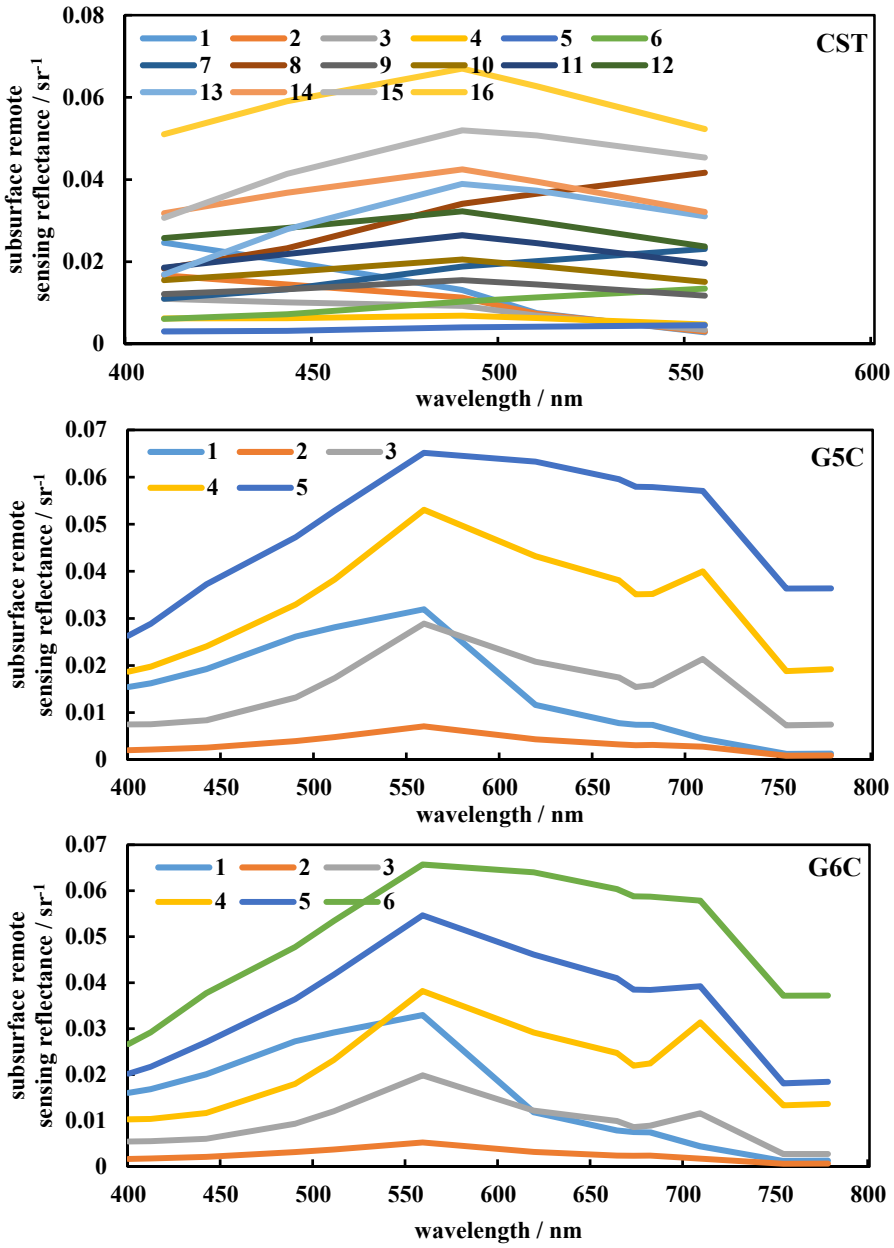

Figure S1. Mean vectors of the AOP-based OWT schemes from previous studies.

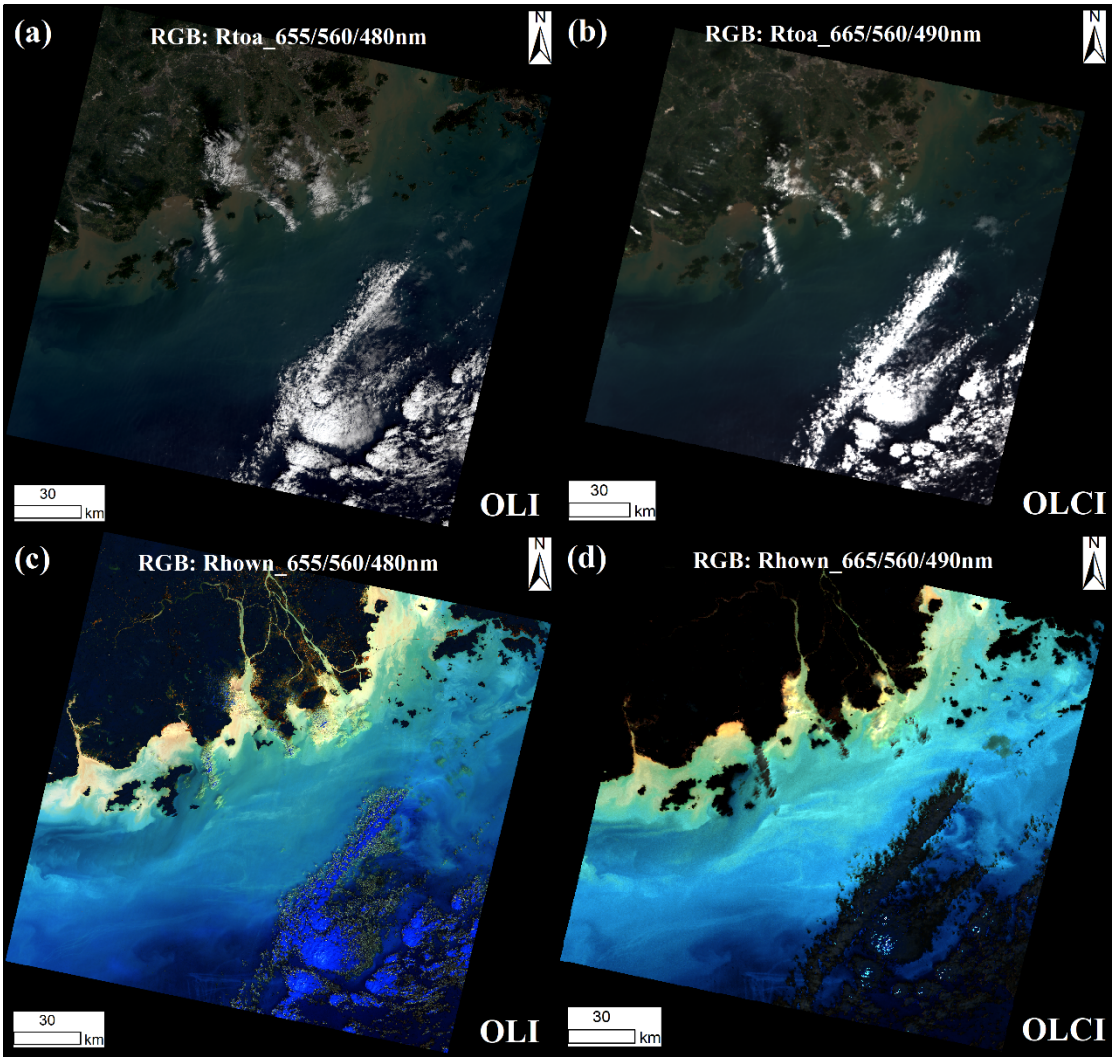

Figure S2. The true color composites of two concurrent (2017/10/23) Landsat-8 OLI and Sentinel-3A OLCI images, before and after the C2RCC atmospheric correction processing. (a) Top of atmosphere radiance (R_{toa}) 655/560/480 nm composite of the raw OLI image; (b) top of atmosphere radiance (R_{toa}) 665/560/490 nm composite of the raw OLCI image; (c) normalized water-leaving radiance (R_{hown}) 655/560/480 nm composite of the OLI image after C2RCC atmospheric correction; (c) normalized water-leaving radiance (R_{hown}) 665/560/490 nm composite of the OLI image after C2RCC atmospheric correction. Note that the OLCI image was georeferenced and resized according to the OLI image.

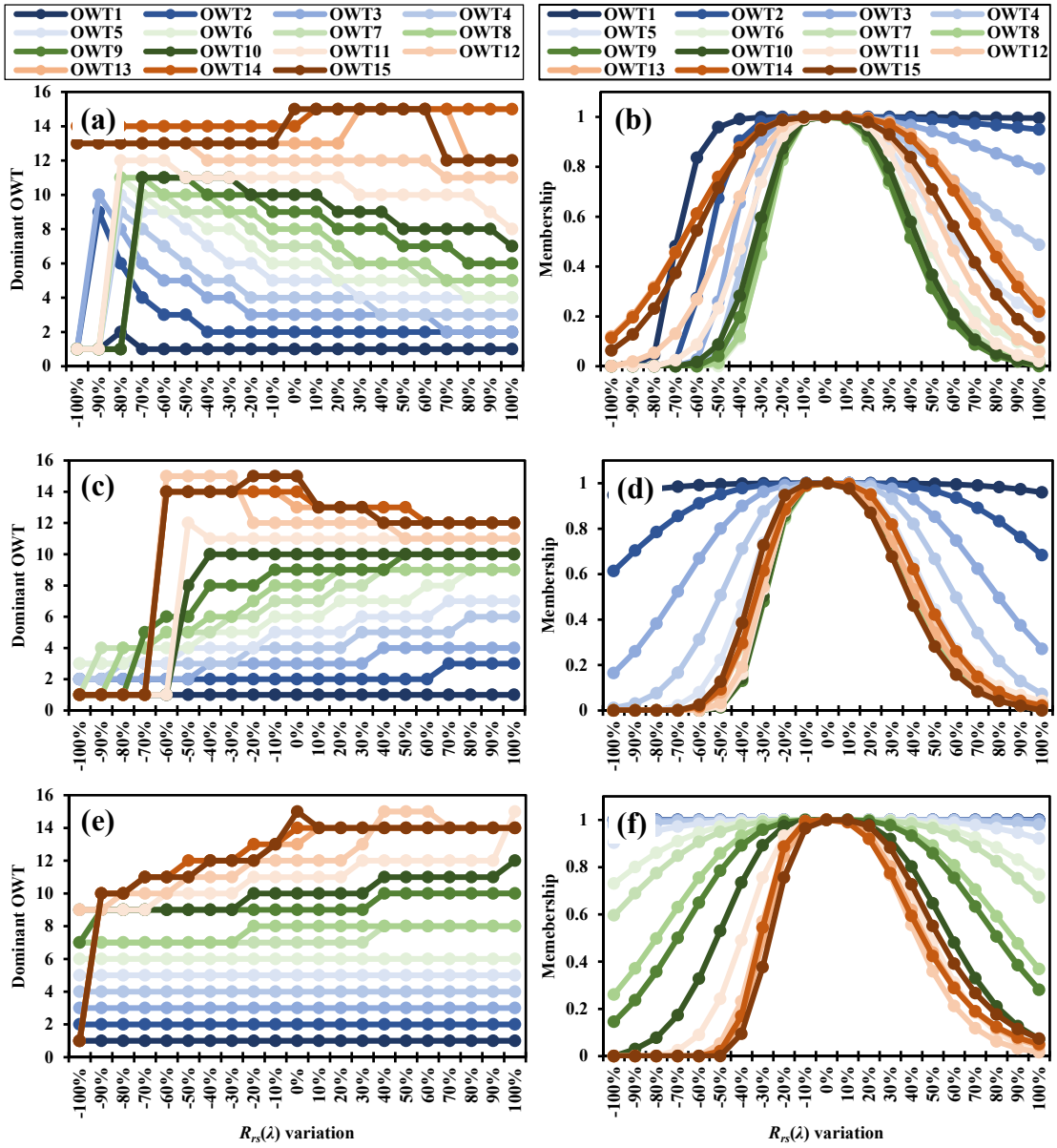

Figure S3. The U-OWT dominant OWT and membership changes of 15 OLI (4 bands) mean $R_{rs}(\lambda)$ vectors under the variations of (a-b) the blue bands (400-500nm), (c-d) the green bands (500-600nm), (e-f) the red bands (600-700nm).

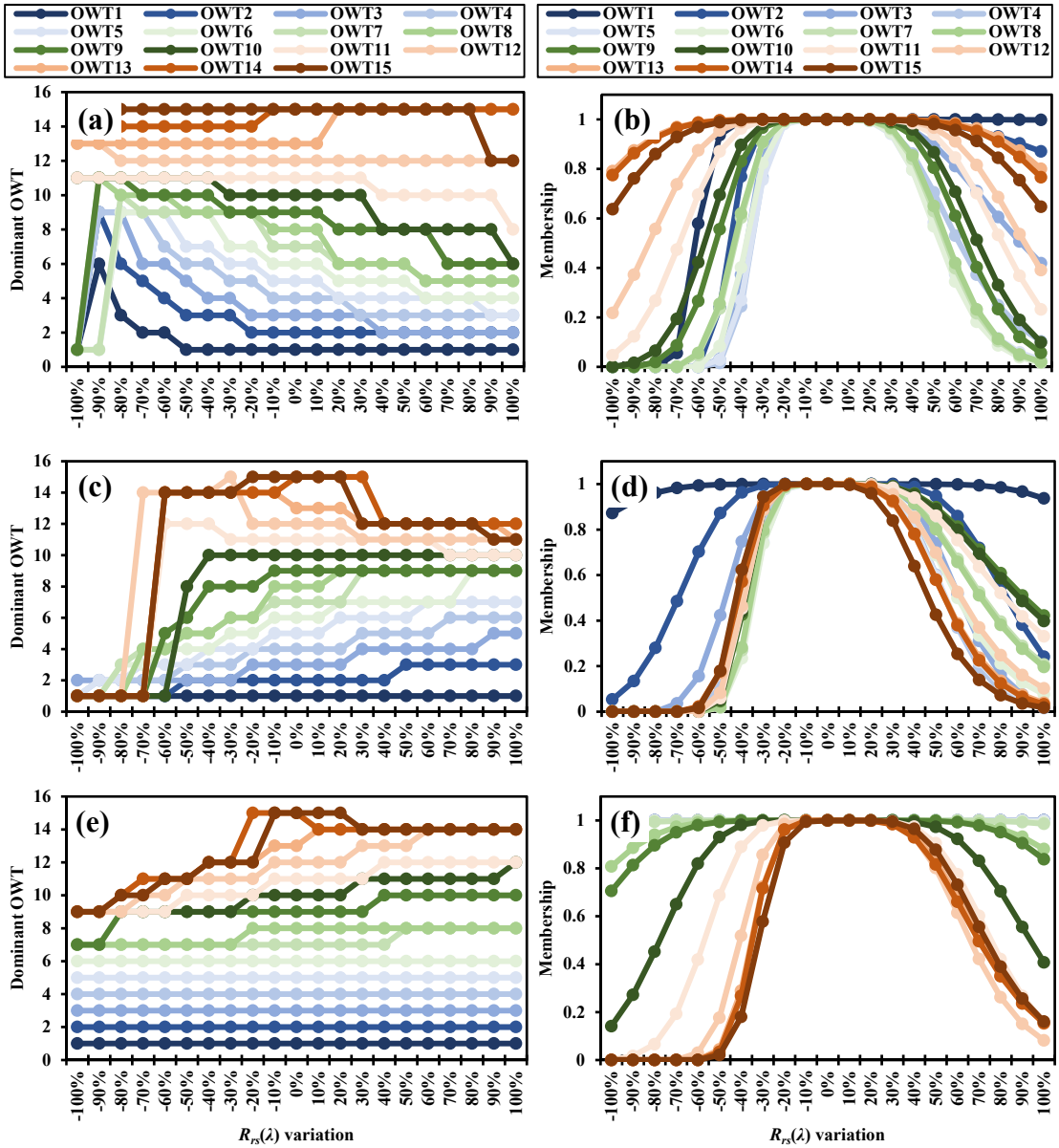

Figure S4. The U-OWT dominant OWT and membership changes of 15 MODIS-Aqua (8 bands) mean $R_{rs}(\lambda)$ vectors under the variations of (a-b) the blue bands (400-500nm), (c-d) the green bands (500-600nm), (e-f) the red bands (600-700nm).

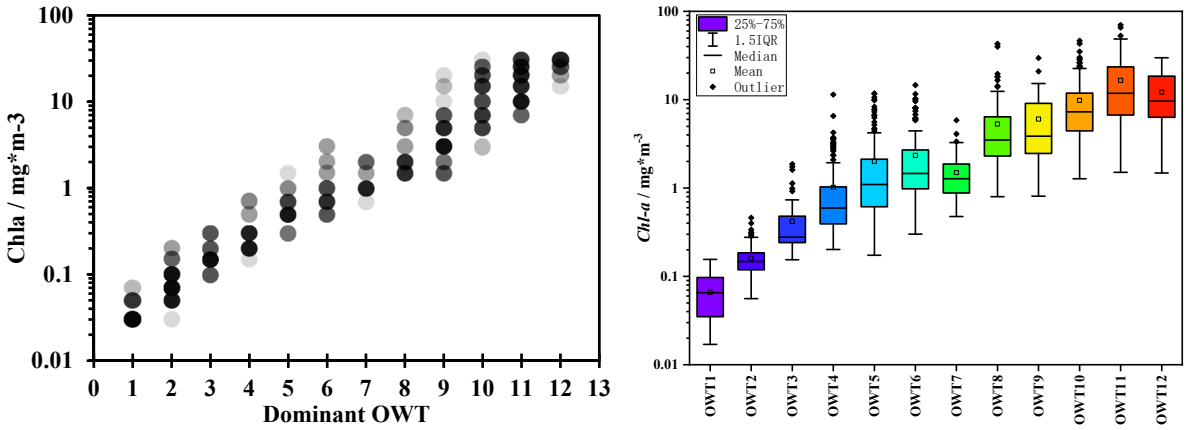

(a) (b)

Figure S5. The relationships between the U-OWT and Chla concentrations. (a) Scatterplot of data pairs of the *Chla* concentrations and the U-OWT dominant OWT from the IOCCG synthetic SeaWiFS convolutional $R_{rs}(\lambda)$ (N = 500). This synthetic data set covers a wide range of natural waters with *Chla* concentration from 0.03 to 30 mg/m^3. The points are plotted with 85% transparency to show the data density. (b) Chla concentration distributions of NOMAD and CCRR in-situ measurements corresponding to different U-OWT dominant OWT (OWT1-OWT12). OWT13/14/15 are not showed here due to the lack of observations.

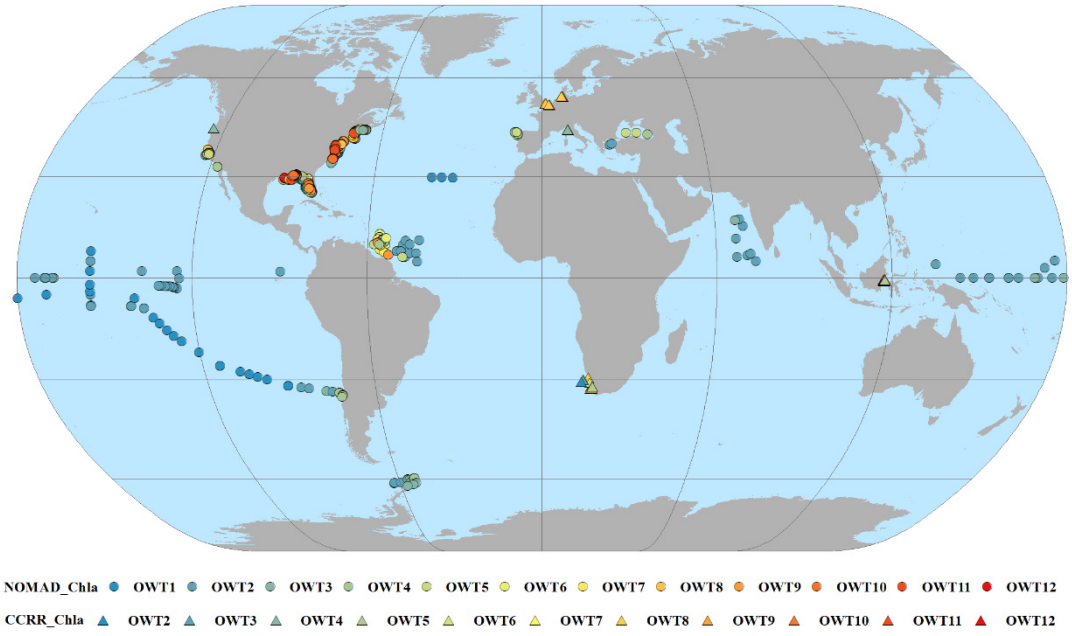

Figure S6. Locations of NOMAD and CCRR in-situ measurements used in this study, and their dominant OWT under the U-OWT context.